Three-Dimensional Investigation of Void Coalescence in Free-Cutting Steel using X-ray Tomography

Seo, Dowon
Department of Mechanical Engineering, Kyushu University

Toda, Hiroyuki
Department of Mechanical Engineering, Kyushu University

Kobayashi, Masakazu
Department of Mechanical Engineering, Toyohashi University of Technology

Uesugi, Kentaro
Japan Synchrotron Radiation Research Institute(JASRI)

他

出版情報：ISIJ International. 55 (7), pp.1483-1488, 2015-07-15. 日本鉄鋼協会
バージョン：
権利関係：© 2015 ISIJ

ISIJ International, Vol. 55 (2015), No. 7, pp. 1483–1488

Three-Dimensional Investigation of Void Coalescence in Free-Cutting Steel using X-ray Tomography

Dowon SEO,[1)]* Hiroyuki TODA,[1)] Masakazu KOBAYASHI,[2)] Kentaro UESUGI,[3)] Akihisa TAKEUCHI[3)] and Yoshio SUZUKI[3)]

1) Dept. of Mech. Eng., Kyushu Univ., Motooka 744, Nishi-Ku, Fukuoka, 819-0395 Japan.
2) Dept. of Mech. Eng., Toyohashi Univ. of Tech., Hibarigaoka 1-1, Toyohashi, Aichi, 441-8580 Japan.
3) Japan Synchrotron Radiation Research Institute, Mikazuki, Sayo, Hyogo, 679-5198 Japan.

(*Received on December 2, 2014; accepted on March 4, 2015*)

Synchrotron X-ray computed tomography has been applied to visualize and quantify the void coalescence leading to ductile fracture in a free-cutting steel. In situ tensile test was carried out and interrupted at different strains in order to observe the sequential damage process. Each void detected by the absorption contrast was sequentially tracked with increasing strain. The results showed that the occurrence frequency of void coalescence was increased exponentially with increasing the strain. Quantitative data obtained by this method was then used to compare and validate the several pre-existing models predicting the void coalescence. Both the Thomason and the Pardoen and Hutchinson models calculated with an average intervoid distance gave a reasonable prediction for large scale coalescence of voids leading to failure.

KEY WORDS: ductile fracture; X-ray tomography; void coalescence; free-cutting steel.

1. Introduction

Ductile damage evolution is driven by plastic deformation which leads to the fracture of most metallic materials. It involves three stages, *i.e.*, the nucleation, growth and coalescence of voids.[1)] The voids may be pre-existing from material processing or nucleated from the second-phase particles via cracking or interface separation during deformation.[2–5)] The void coalescence process is a complex function of the material properties, the local stress state and the void geometry including the relative orientation of the intervoid ligament with respect to the principal loading direction.[1,5)] With technological advances in hardware and software of X-ray tomography technique, the void coalescence can be clearly observed during in situ tensile test,[5–7)] as well as the the nucleation and growth of voids.[8,9)]

Recently, employing X-ray tomography has extended to study on the void coalescence events in steels. Weck *et al.*[6)] has used an artificial sample containing array of laser-drilled, quasi-spherical holes to analysis the void coalescence in a controlled manner. In their study, the coalescence event was well captured using X-ray tomography. Thomason model[1,10)] for the void coalescence gave good predictions for the pure copper sample containing holes coalescing normal to tensile axis. In the case of study on the Glidcop sample including alumina particles, however, the Thomason model has failed to predict coalescence; this is primarily due to lack of sufficient consideration about secondary void nucleation caused from the inclusions in the sample.[6)] Hosokawa *et al.*[11,12)] extended the model studies on the coalescence event in the copper sample including more complex array of artificial holes and revealed that both the Thomason model and the Pardoen and Hutchinson (PH) model[13)] give good prediction for voids coalescing normal to tensile axis. In the case of alloys amenable to strain hardening such as brass, the strain starting the coalescence event was in better agreement with the PH model.[7)] High strain hardening suppressed plastic flow in the intervoid ligaments and led to late void linkage.

Most studies mentioned above are limited to the inclusion-free or unconsidered,[14–17)] the homogeneous[9)] and the model materials embedding artificial damages[6,7,11,12)] for easy estimation. Concerning the final stage of damage process leading to a ductile fracture, especially, it is difficult to obtain quantitative data because of the stochastic nature of void coalescence, the intricate clustering patterns of coalescing voids, and the algorithmic difficulty in tracking of them in sequence. Furthermore, the coalescing takes place by a relatively small increment of strain at high strain. The artificial voids, therefore, have been employed in many studies to simplify the analysis of coalescence phenomenon. However, an eager desire to observe the void coalescence in the commercial steels is still remained, as well as the void nucleation and growth. The quantitative data on the damage evolution of the entire void population, in particular, is valuable to making the failure predictions more accurate.

In this work, the damage evolution in a free-cutting steel was studied in situ by combined a tensile test and the tomographic observation to better understand the void coalescence during ductile deformation. Synchrotron X-ray

* Corresponding author: E-mail: seodwn@gmail.com
DOI: http://dx.doi.org/10.2355/isijinternational.55.1483

absorption tomography has been applied to visualize and collect quantitative three-dimensional (3D) information on the damage evolution. Quantitative data obtained by this method was then used to compare and validate the several void coalescence models.

2. Experimental Procedure

2.1. Material

A commercial free-cutting steel, JIS SUM24L which has a chemical composition (wt.%) of 1.1 Mn, 0.32 S, 0.28 Pb, 0.08 C, 0.075 P and balance Fe was used. Manganese sulfides (MnS), which are added to ferrite matrix to enhance the machining performance, were elongated in rolling direction (RD) of an extruded rod and not uniform in size as well as in their spatial distribution (see **Fig. 1** in Ref. 18)). The volume fraction and average diameter of the MnS were found to be about 1.1% and 8.3 μm, respectively. The ferrite grains of about 50 μm as main matrix and the pearlites which stretched and oriented to RD were observed. Leads were also detected around tails of some MnS inclusions, but their effect on the damage evolution was not considered in this study because of their low volume fraction of 0.02%.

2.2. In Situ Tensile Test

A flat specimen of 600 μm in thickness was machined from the round bar of 25 mm in diameter, where the tensile loading axis to be corresponded to RD. Its cross section was 600×600 μm^2. Tensile test was carried out at constant crosshead speed of 0.0005 mm/s at room temperature using a specially designed in situ equipment installed on a highly precise rotation stage described in the references.[19,20] During the in situ experiments, the specimen was deformed in tension and the test interrupted at different strain levels (10 steps up to the strain of 0.64) with planned interval in order to acquire tomograms sequentially (see **Fig. 3** in Ref. 18)).

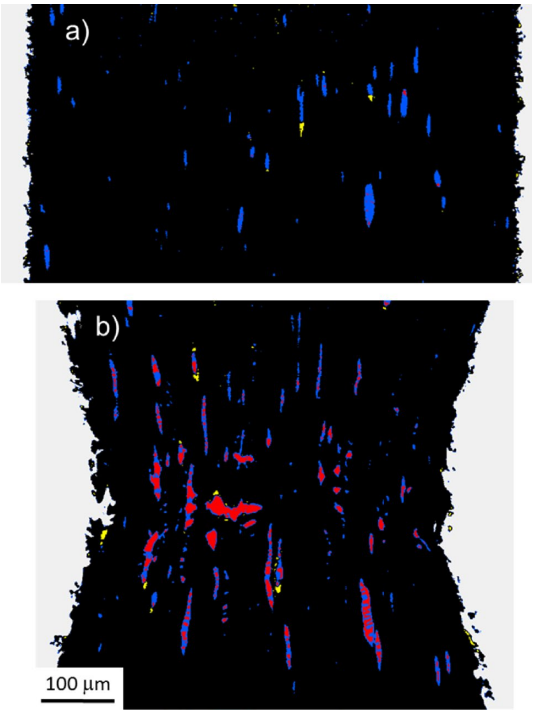

Fig. 1. Side view of ROI segmented by LAC, a) before and b) after loading. Red indicates voids, blue MnS, yellow Pb and black a matrix. (Online version in color.)

2.3. X-ray Tomography

X-ray tomography was conducted at the undulator beamline BL20XU of SPring-8, Japan Synchrotron Radiation Research Institute. A monochromatic X-ray beam of 40 keV was used with a beam source-to-sample distance of 80 m. A sample-to-detector distance was set to 65 mm. A 2D-CCD (C4880-41S, Hamamatsu Photonics, Japan) of 4 000×2 624 pixels was used with a 10 μm thick scintillator of Lu_2SiO_5:Ce and its effective field of view was about 720×600 μm. Isotropic voxels with 0.5 μm edges in the reconstructed volume were obtained from 2D projection radiographs via the convolution back projection algorithm.

The stack of slice images with a 16-bit gray depth which corresponds to the linear absorption coefficient (LAC) of the materials was converted into 8-bit images. The LAC was also used to determine the lower and upper thresholds for segmenting out the voids from the matrix after 8-bit conversion, as shown in Fig. 1.

After the segmentation process, 3D volumetric image was rendered to evaluate a spatial distribution of the voids.

The region of interest (ROI) of 696 μm (W)×726 μm (D)×548 μm (H) at final step of tomography scan (696×726×332 μm^3 at unloading state) was cut off from the center of the stack. A 3D labeling algorithm was applied to the binarized images, and the labelled voids in the ROI were tracked with an increase of strain. Then, their microstructural features such as the position of gravity center, the volume and so on were measured. The details of the tracking algorithm are described in the references.[18,21,22]

3. Results and Discussion

Some of the grown voids were coalesced at certain point of strain enough to extend the growing and connect to each other. It is visible of the sequential necking of the ligament between the adjacent voids down to a line by tomographic observation and the necking with secondary void nucleation on some occasions. **Figs. 2**(a), 2(b) and 2(c) show radiographs taken at the strain of 0.29, 0.50 and 0.64, and their tomographic reconstructions presenting the sequence of void coalescence (red in color) in 3D are also shown in following Figs. 2(d), 2(e) and 2(f), respectively. The voids are clearly visible. The fully grown voids linked up with the adjacent voids and then clustered together. In Figs. 2(d), 2(e) and 2(f), the matrix is transparent and only the outer surface of the ROI is visualized in a semitransparent mode. The MnS inclusions elongated to tensile direction are blue in color. Numerous inclusions were seen in the 3D images, but the volume fraction of the pre-existing inclusions measured was only 1.1% as mentioned previously which is much smaller than expected from these figures.

As a typical example, a 3D rendering of three adjacent voids extracted from the tomographic reconstruction is presented in Fig. 3. It was a same void cluster shown at the center of Fig. 2(b) and tilted slightly at an angle to present a first linking clearly. It is possible to identify the voids related to ligament linkage as well as their interactions and

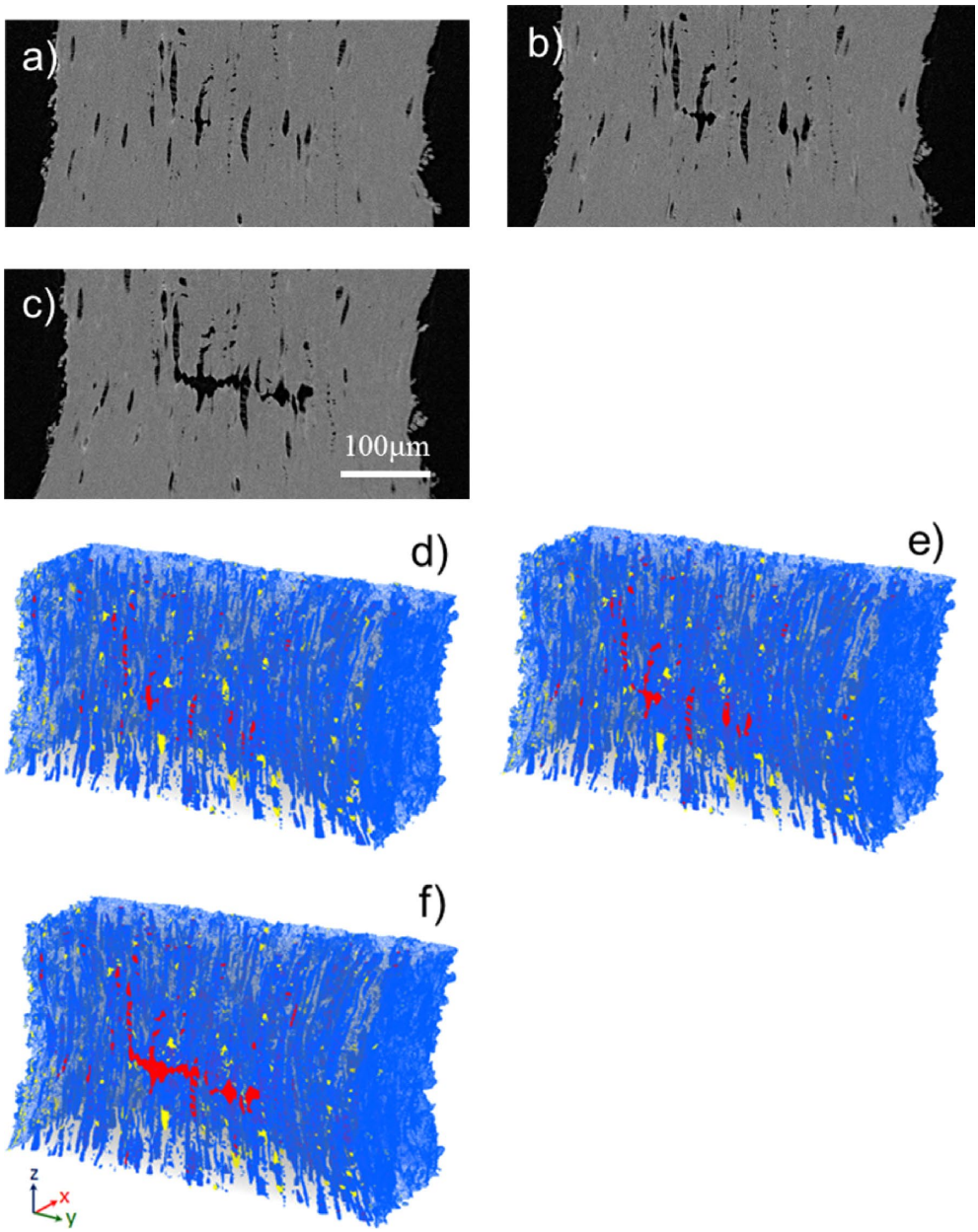

Fig. 2. Radiographs taken at the strain of a) 0.29, b) 0.44 and c) 0.64, and their tomographic reconstructions showing the sequence of void coalescence (red in color): 3D volumetric images in d), e) and f) correspond to a), b) and c), respectively. (Online version in color.)

to trace them individually by virtue of in situ tomographic observation. From sequential observing the volumes of three voids shown in Fig. 3, Void #2 linked up with Void #1 at the strain of 0.44 and then started to grow in one united body with increasing strain, as shown in **Fig. 4**(a). It can also be recognized by tracking the length of the Void #2 in 3D. This linkage took place in transverse direction which triggered a sudden increase in the transverse length at $\varepsilon=0.44$, as shown in Fig. 4(b). In striking contrast to the increase in the transverse length of the void, a relatively small increase of the void length in tensile direction was observed at the same strain.

Extending considerations into the entire void population in ROI, the volume fraction of the voids related to the coalescence was exponentially increased with increasing strain as shown in **Fig. 5**(a). This volume fraction evolved uninterruptedly from the beginning of the deformation and it could be related to the continuous increase of the occurrence frequency of the void coalescence f_c (number of occurrence of void coalescing events per unit volume) shown in **Fig. 6** which was increased exponentially with increasing the strain. Of course, this evolution could be also involved in the own growth of the coalescing voids at once but a predominant evolution is based on the clustering of them. It should be aware that this evolution of the volume fraction shown in Fig. 5(a) is only for the voids which already coalesced or will coalesced in coming deformation. The volume fraction of the coalescing voids just before fracture (at $\varepsilon=0.64$) was only 0.74% of the whole volume of ROI and only about 20% of the volume of the entire void population was related to coalescing. It was realized that lesser amount of voids than expected was coalesced and clustered together in a concentrated area which was directly related to a final fracture.

It is also worth considering the length evolution of the entire coalescing voids in ROI because the dimensional

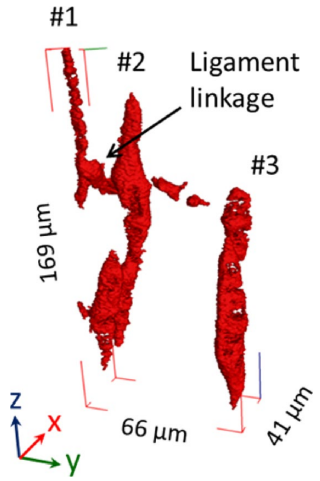

Fig. 3. Close-up of three adjacent voids showing typical coalescing sequence. A rendering image was taken at the strain of 0.44. (Online version in color.)

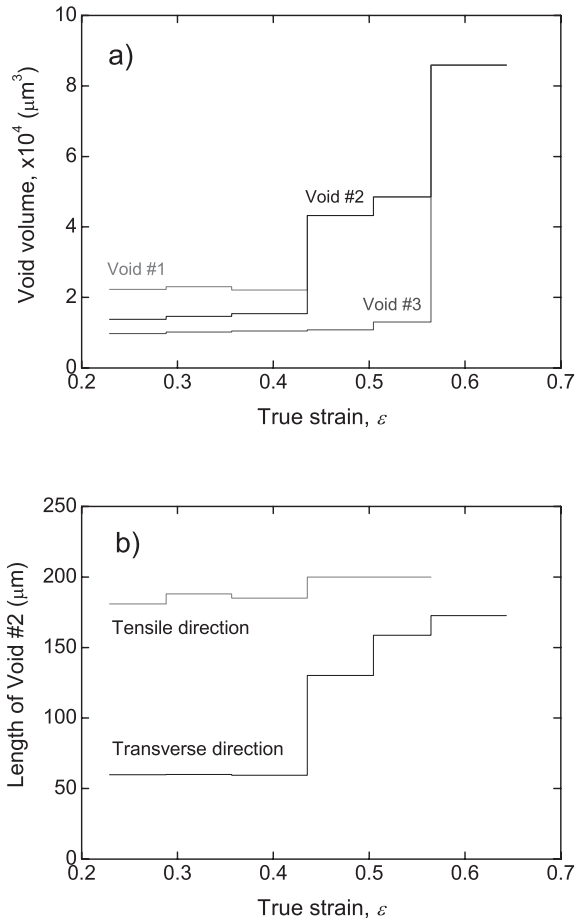

Fig. 4. Evolution of a) the volume of three voids and b) the length of Void #2 as a function of strain.

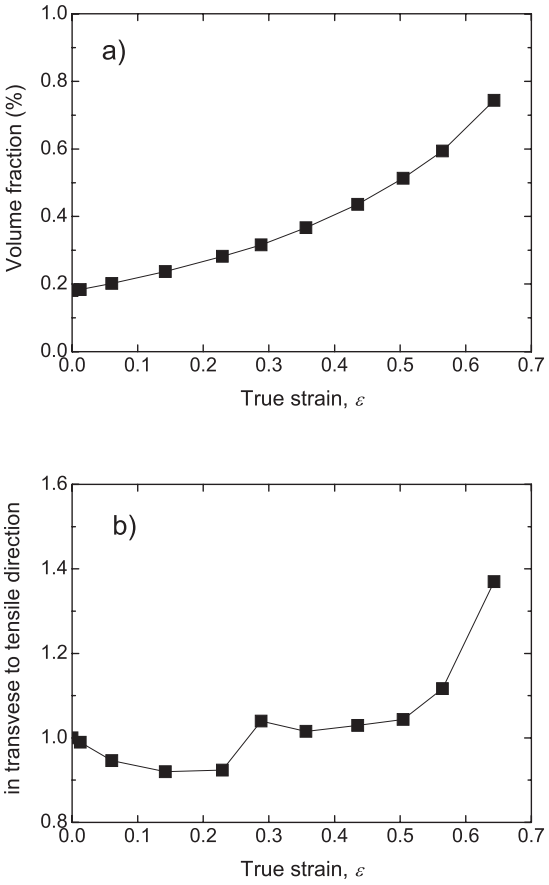

Fig. 5. Evolution of a) the volume fraction of entire coalescing voids and b) the normalized ratio of the average void length in transverse direction to one in tensile direction.

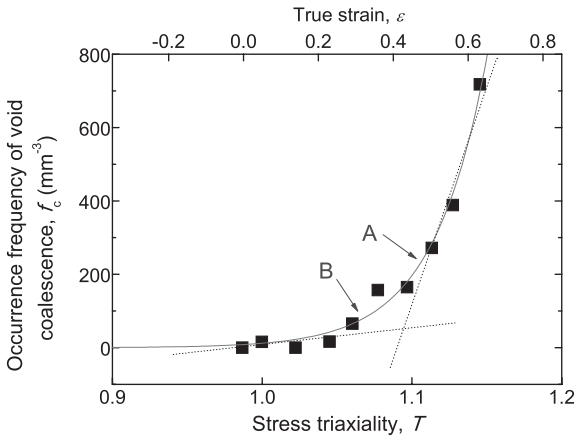

Fig. 6. Relationship between occurrence frequency of void coalescence and stress triaxiality.

information of the voids such as the void length or the length ratio is one of the important parameters concerning prediction of a coalescing event.[1,10,13] Fig. 5(b) shows the evolution of the normalized ratio of the average void length in transverse direction $2b_m$ to one in tensile direction $2a_m$. The ratio of b_m/a_m at each strain step was normalized to one at the unloading state ($\varepsilon=0$) to allow easier comparison between them. Considering the low ratios at the beginning of deformation (less than $b_m/a_m=1$), the void growth in tensile direction was dominant up to the strain of 0.29. The a_m, that is, further increased with increasing the strain compared to the b_m because the b_m values were almost constant at this regime ($2b_m=9.42-9.57$ μm). From the strain of 0.56, the transverse direction turned into a predominant direction in the void evolution which represents a horizontal wholescale coalescence leading to a final fracture of specimen.

Based on the experimental observation shown in Fig. 6, it is not easy to define an onset of void coaclescing in terms of a specified value of strain due to the continuous occurrence of coalescing events over all strain regimes.

Additional information such as Fig. 5(b) and a comparative consideration with several established prediction models which enables a better understanding of the parameters controlling the void coalescence could be of assistance to more accurate estimation of the onset point. The Thomason model[1,10] and the PH model[13] were considered for the onset comparison with the experimental results due to reasonable validity of their predictions with tomography experiments demonstrated in several previous studies.[6,7,11,12] The Thomason model for uniaxial tensile deformation predicts that the onset of the void coalescence takes place when the following equation is verified:[1]

$$\left(\frac{0.1}{(a/e)^2}+\frac{1.2}{\left(\frac{b}{b+e}\right)^{1/2}}\right)\frac{1}{(1-P_0)}\left(1-\left(\frac{3\sqrt{\pi}P_0}{4}\right)^{2/3}\left(\frac{b}{b_0}\right)^2\right)exp(\varepsilon) = \frac{\sigma_m}{Y}+\frac{2}{3} \quad \text{..... (1)}$$

where, a and b are half lengths of voids in tensile and transverse directions, respectively. b_o is half an initial void length in transverse direction, e half an intervoid distance, σ_m the average stress, Y a uniaxial yield stress and P_0 an initial packing density of void in a restricted volume which can be extracted from tomograms. Considering a spherical void in a cubic unit cell which is an assumed premise of the Thomason model, the intervoid distance $2e$ can be expressed with half an initial length a_o in tensile direction as following form:

$$e = a_0\left(3\sqrt{\frac{\pi}{6P_0}}exp\left(-\frac{1}{2}\varepsilon\right)-\frac{b}{b_0}\right) \quad \text{..... (2)}$$

The Thomason model was originally proposed for the coalescing between only two voids. To extend its scope into the entire void population in ROI, first of all, the average values of the geometric dimensions of the voids, a and b were considered to calculate the average value of intervoid distance e_{ave} at each strain level from Eq. (2). The minimum value of intervoid distance e_{min} was also considered as shown in **Fig. 7**, which was calculated using the maximum a and b at each strain. Because it is believed that the pair of voids coming closest to each other in ROI would tends to start linking as the first onset of the coalescence at certain strain level. The minimum distance, e_{min} reached the zero at the strain of about 0.37 comparing about 0.53 for the e_{ave}.

Left-hand side (LHS) of Eq. (1) calculated with both e_{ave} and e_{min} were plotted in **Fig. 8** against the right-hand side of Eq. (1) and their intersections gave the onset strains of the void coalescence. The coalescing strain was 0.48 in the case of the Thomason model calculated with the e_{ave}. It corresponds to a point of A in Fig. 6, which is positioned between the tomography scan points of ε=0.44 and ε=0.50, and in the beginning regime of a rapid growth of the f_c. Regarding the strain of 0.44 as the onset point of the large scale coalescence from a series of results, the difference of the onset strain between the prediction and the experiment was 0.04 and 9% overestimated. This difference is likely to be due to the secondary population of voids nucleation among the primary voids as discussed in the other study in the series (see **Fig. 9**(b) in Ref. 18)). The secondary voids could accelerate the coalescence of voids resulting in reduction of the coalescence strain.[23] Allowing for estimation with average values of numerous voids in ROI, however, it gives a reasonable prediction for large scale coalescence of voids leading to failure. As can be seen in Fig. 5(b) again, growing void length in the transverse direction was also remarkable from the strain of 0.48 predicted by Thomason model with the e_{ave}. It represents that the void linkage takes place from that point in the direction normal to tensile loading and micro cracks propagate to failure, as shown in Figs. 2(b) and 2(e).

On the other hand, in the case of considering the e_{min} value, the predicted onset strain was 0.30 and could be correspond to the point of B in Fig. 6, just diverging from a stagnant state in the occurrence frequency of void coalescing events. From that point, the normalized ratio of the void length was also turned over to more than 1, as shown in Fig. 5(b), *i.e.*, the void length in transverse direction started to grow dominantly together with microscale coalescing between isolated small voids. From considering these two results, it is acceptable to draw a conclusion that the Thomason model with the e_{min} predicts the onset of the void coalescence in microscale level. To be precise, as can

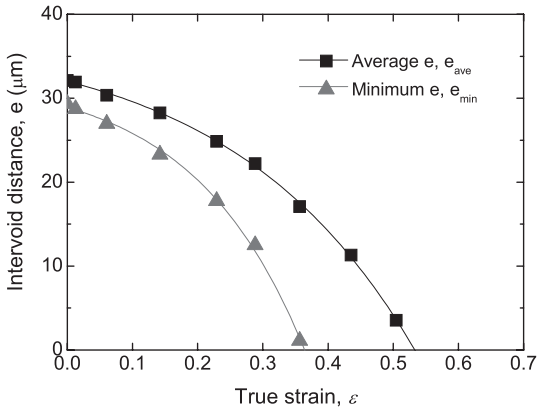

Fig. 7. Evolution of average and minimum values of the intervoid distance e, calculated by using average and maximum values of void geometric dimensions, respectively.

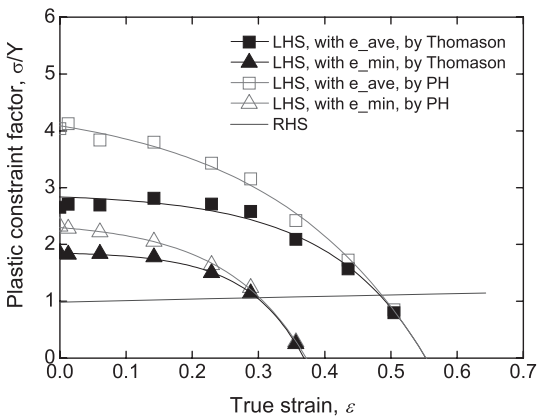

Fig. 8. Comparison of two coalescing strain predictions calculating with the average value e_{ave} and the minimum value e_{min} of intervoid distance.

be seen in Fig. 5(b), the void coalescing events were also observed at $\varepsilon=0.06$ ($T=0.99$) and $\varepsilon=0.23$ ($T=1.05$) even though in a very limited number. It could be due to a large number of soft inclusions inside specimen. They would be likely to be linked together even after smaller deformation and even at T of less than 1. Further studies are needed to better understand the specific nature of the relationship between the soft inclusions and the damage evolution, especially for abnormal void coalescing.

The influence of the strain hardening on the coalescence was also studied with the model proposed by PH.[13] To take this effect into account, they proposed replacing the constant 0.1 and 1.2 in the LHS of Eq. (1) by $\alpha(n)$ and $\beta(n)$, respectively.

$$\left(\frac{\alpha(n)}{(a/e)^2}+\frac{\beta(n)}{\left(\frac{b}{b+e}\right)^{1/2}}\right)\frac{1}{(1-P_0)}\left(1-\left(\frac{3\sqrt{\pi}P_0}{4}\right)^{2/3}\left(\frac{b}{b_0}\right)^2\right)exp(\varepsilon)=\frac{\sigma_m}{\bar{\sigma}}+\frac{2}{3} \quad \text{..... (3)}$$

where, $\bar{\sigma}$ is a local effective stress and was assumed to be equal to the equivalent stress σ_{eq} in this study. It could be a quite appropriate assumption if the voids are spherical or elongate in dominant strain direction, because the stress triaxiality and the plastic constraint induced from the voids are negligible.[7] Both $\alpha(n)$ and $\beta(n)$ are functions of the strain hardening exponent n. $\alpha(n)$ is given by the following relationship while $\beta(n)$ is defined to be almost constant equal to about 1.24:

$$\alpha(n)=0.1+0.217n+4.83n^2, \qquad (0\le n\le 0.3) \quad \text{.... (4)}$$

When $n=0$ in Eqs. (4), (3) becomes to be same with Eq. (1), *i.e.*, the Thomason model. For the sake of high contrast, an upper limit of $n=0.3$ was chosen to maximize the strain hardening effect on the onset of the void coalescence for the material studied in this study.

As can be seen in Fig. 8, at a lower strain regime, the LHS values of Eq. (3) were quite different from those given by the Thomason model when the strain hardening effect was considered. However, the difference was gradually reduced with increasing strain. The PH model with both the e_{ave} and e_{min} consideration, therefore, gave almost same values of the onset strain of the void coalescence with those predicted by the Thomason model which assumes the matrix to be strain hardening-free. This could be due to a rapid reduction in the strain hardening rate of the matrix at high strain regime, as discussed in the other study in the series (see Fig. 3 in Ref. 18)). It was also observed in several previous works with different types of steels.[6,7,11] In the case of the material used in this study, therefore, it can be concluded that the effect of the strain hardening on the void coalescence is negligible if the deformation goes up to high strain regime.

4. Conclusion

Void coalescence leading to ductile fracture in free-cutting steel were successfully visualized and quantified using an in situ high resolution synchrotron X-ray computed tomography. From the sequential observation of void coalescing by tomography, the occurrence frequency of void coalescence was increased exponentially with increasing the strain. The models predicting void coalescence were validated and discussed based on quantitative observation. Both the Thomason and the PH models calculated with an average intervoid distance e_{ave} gave a reasonable prediction for a large scale coalescing of voids leading to failure. Introducing a minimum intervoid distance e_{min}, both the models were able to predict the onset of microscale void coalescence.

Acknowledgments

Authors gratefully acknowledge that this work was undertaken as a technical research aid project "Breakthrough in research on steel by realizing 4D imaging" of the ISIJ Innovative Program for Advanced Technology.

REFERENCES

1) P. F. Thomason: *J. Inst. Met.*, **96** (1968), 360.
2) L. Babout, E. Maire, J. Buffiere and R. Fougeres: *Acta Mater.*, **49** (2001), 2055.
3) L. Babout, E. Maire and R. Fougeres: *Acta Mater.*, **52** (2004), 2475.
4) E. Marie, C. Bordreuil, L. Babout and J. C. Boyer: *J. Mech. Phys. Solids*, **53** (2005), 2411.
5) A. Weck, D. S. Wilkinson and E. Maire: *Mater. Sci. Eng. A*, **488** (2008), 435.
6) A. Weck, D. S. Wilkinson, E. Maire and H. Toda: *Acta Mater.*, **56** (2008), 2919.
7) A. Hosokawa, D. S. Wilkinson, J. Kang, M. Kobayashi and H. Toda: *Int. J. Fract.*, **181** (2013), 51.
8) E. Marie, S. Zhou, J. Adrien and M. Dimichiel: *Eng. Fract. Mech.*, **78** (2011), 2679.
9) D. Fabregue, C. Landron, O. Bouaziz and E. Marie: *Mater. Sci. Eng. A*, **579** (2013), 92.
10) P. F. Thomason: *Acta Metall.*, **33** (1985), 1087.
11) A. Hosokawa, D. S. Wilkinson, J. Kang and E. Maire: *Acta Mater.*, **61** (2013), 1021.
12) A. Hosokawa, D. S. Wilkinson, J. Kang and E. Maire: *Acta Mater.*, **60** (2012), 2829.
13) T. Pardoen and J. Hutchinson: *J. Mech. Phys. Solids*, **48** (2000), 2467.
14) E. Marie, O. Bouaziz, M. D. Michiel and C. Verdu: *Acta Mater.*, **56** (2008), 4954.
15) C. Landron, O. Bouaziz, E. Marie and J. Adrien: *Scr. Mater.*, **63** (2010), 973.
16) A. Bareggi, E. Maire, O. Bouaziz and M. D. Michiel: *Int. J. Fract.*, **174** (2012), 217.
17) C. Landron, E. Maire, O. Bouaziz, J. Adrien, L. Lecarme and A. Bareggi: *Acta Mater.*, **59** (2011), 7564.
18) D. Seo, H. Toda, M. Kobayashi, K. Uesugi, A. Takeuchi and Y. Suzuki: *ISIJ Int.*, **55** (2015), 1474.
19) H. Toda, T. Ohgaki, K. Uesugi, M. Kobayashi, N. Kuroda, T. Kobayashi, M. Niinomi, T. Akahori, K. Makii and Y. Aruga: *Metall. Trans. A*, **37** (2006), 1211.
20) M. Kobayashi, H. Toda, A. Takeuchi, K. Uesugi and Y. Suzuki: *Mater. Charact.*, **69** (2012), 52.
21) M. Kobayashi, H. Toda, Y. Kawai, T. Ohgaki, K. Uesugi, D. S. Wilkinson, T. Kobayashi, Y. Aoki and M. Nakazawa: *Acta Mater.*, **56** (2008), 2167.
22) H. Toda, E. Maire, Y. Aoki and M. Kobayashi: *J. Strain Anal. Eng. Des.*, **46** (2011), 549.
23) D. Lassance, D. Fabregue, F. Delannay and T. Pardoen: *Prog. Mater. Sci.*, **52** (2007), 62.